Materials Today Communications 35 (2023) 106054

Contents lists available at ScienceDirect

Materials Today Communications

journal homepage: www.elsevier.com/locate/mtcomm

Extreme flexibility and unusual piezomechanical properties of zinc-alkyl-based metal-organic frameworks: A first principles study

Mustafa Erkartal

Abdullah Gül University, Department of Nanotechnology Engineering, 38080 Kayseri, Turkey

ARTICLE INFO

Keywords:
Metal-organic frameworks
High pressure
Negative linear compressibility
Zero
Linear compressibility
Mechanical metamaterial

ABSTRACT

The behavior of three Zn-alkyl-based MOFs, ZnGA (Zn-Glutarate), ZnAA (Zn-Adipate), and ZAG-4 (Zinc Alky Gate), under hydrostatic compression has been investigated using first-principles DFT simulation, which has proven its reliability in previous studies. Due to the lack of the high pressure experimental data for ZnGA and ZnAA, the reliability of the simulation parameters was tested by taking ZAG-4, whose structural flexibility has been previously reported experimentally and computationally, as a benchmark. All three structures were found to exhibit elastic deformation under pressure up to 15 GPa, due to the flexibility of the alkyl chains that allow the structures to move without disrupting the metal-ligand coordination. Interestingly, the structures exhibit different mechanical properties, with ZAG-4 showing negative linear compressibility (NLC), ZnGA showing positive linear compressibility (PLC), and ZnAA showing zero linear compressibility (ZLC). The NLC in ZAG-4 is attributed to the proton transfer between phosphonate oxygen and water in the structure as previously reported, while the ZLC in ZnAA is due to a dumbbell-like structural motif formed by substructures displaying both NLC and PLC.

1. Introduction

Metal-organic frameworks (MOFs) have attracted a great deal of attention over the last two decades owing to the fascinating range of structures and properties these materials show [1]. The majority of these studies have focused on applications requiring high surface fields such as gas storage/separation [2–5], catalysis [6–8], and electrochemical [9–13] due to the high porosity of MOFs. Recently, however, the extraordinary electronic [14,15], optical [16–18], and mechanical properties exhibited by MOFs, especially those containing extensive metal-oxygen-metal-connectivity have also received much attention. Among them, the study of frameworks that can experience reversible phase transitions in response to physical stimuli like compression [19], guest exchange [20,21], and/or framework activation [22] is of particular interest.

Porous MOFs with high structural dynamics provide special opportunities for adsorption and selective separation because they can enclose a guest, promoting mutual intermolecular interactions and molecular recognition. The structural flexibility of MOFs in this group has been explained by different mechanisms in the literature. For example, the flexibility of several ZIFs was ascribed to the rotation of their imidazolate linkers called as swing effect or gate-opening phenomenon [23,24]. The breathing effect, which is a reversible phase transition under an external stimulus, observed in the MIL-53 series was explained by the significant changes in the unit cell caused by the varying degrees of rotation of the phenylene ring about its C-C axis [25,26]. The breathing effect in DUT-49, which displays negative gas adsorption, is explained by the deformation of the ligand caused by the rotation of the metal node [27].

Obviously, the flexibility of such MOFs is directly related to the limited degrees of freedom that carboxylate or azole-based ligands with rigid benzene backbone have in the crystal. Therefore, the incorporation of organic ligands with high degrees of freedom into the MOF structure can result in crystals with unusual structural properties. On the other hand, usage of flexible ligands with a high degree of conformational freedom as building unit may lead to the formation of unexpected structures during the crystallization process [28,29]. Therefore, the crystal structures of MOFs produced from flexible ligands are highly dependent on the synthesis conditions, namely temperature, reaction time, concentration, and pH [30]. Also, the resulting structures are often either dense or have a very low accessible surface area [31,32]. All these factors hinder the synthesis of rationally designed and predictable MOF architectures from flexible ligands. Therefore, when compared to their rigid counterparts, MOFs with flexible ligands have been less studied in

E-mail addresses: mustafa.erkartal@agu.edu.tr, merkartal@mail.com.

https://doi.org/10.1016/j.mtcomm.2023.106054
Received 8 March 2023; Received in revised form 10 April 2023; Accepted 21 April 2023
Available online 23 April 2023

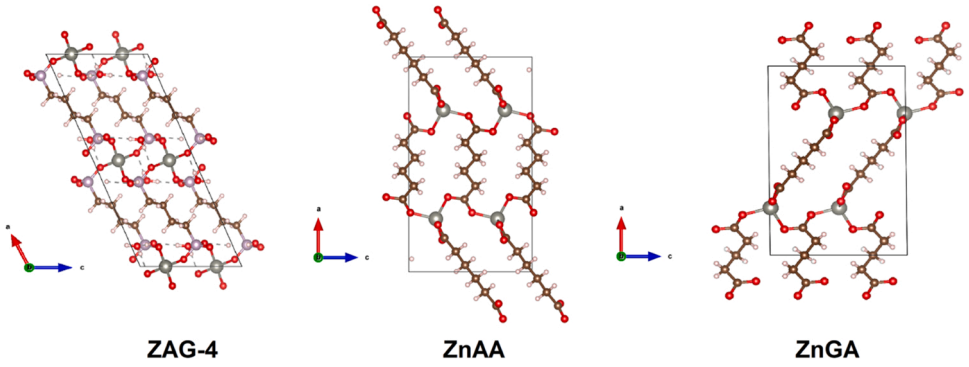

Fig. 1. Crystal structures of ZAG-4, ZnAA and ZnGA. (Zn:grey; P:purple; C:brown; O:red; H:white).

the literature.

The incorporation of flexible structural units may provide molecular systems with potential advantages despite the aforementioned disadvantages may be encountered in the synthesis. In their systematic study, Alberti et al. [33] showed that the interlayer distance could be easily modulated almost continuously by increasing the number of carbon atoms in the alkyl chain by synthesizing Zr-alkyl phosphonate compounds with different lengths of alkyl chains. More interestingly, these compounds exhibit reversible elongation and shortening property of interlayer distance, called as accordion effect, depending on the amount of solvent exit in the interpillar space owing to adopting different conformation of nonrigid alkyl ligands. Reinsch et al.[32] synthesized a novel Al-MIL-53 analogue by using adipic acid as linker. The resulted framework, MIL-53-ADP, exhibits a breathing behavior only upon dehydration and rehydration unlike its aromatic counterpart. The driving force behind this phenomenon is assigned to the change of linker length due to the conformational adaptation in the framework as in Zr-phosphanates. A similar solvent-dependent phase transition was also reported Cu-glutarate based pillared MOFs [34]. Moreover, one of these structures shows a gate-opening property accompanied with a phase change during CO_2 adsorption. Underlying mechanism of the phase change in these materials is ascribed to a direct gauche–gauche enantiomeric conversion. As well as phase transitions induced by a guest molecule, phase transitions under direct hydrostatic pressure for alkyl-based MOFs were also reported. For example, Gagnon et al.[35] experimentally showed that, ZAG-4, a Zn-alkyl phosphanate MOF, is extremely compressible with reversibility up to 10 GPa since the alkyl chains act as a spring to stabilize the compression of the system allowing for large distortions without any bond breaking. In their further joint study [19], they showed that ZAG-4 and ZAG-6 display negative linear compressibility at high pressure because of a structural change linking a reversible proton transfer between an included water molecule and the linker's phosphonate group. Recently, Serre et al.[36] reported that designed MOFs exhibit different structural dynamics toward external stimuli such as temperature or guest molecule depending on the bond stretching and rotation/bending degree of freedom of the linker.

Clearly, our knowledge of the structural dynamics of alkyl-MOFs is based on very limited reports. Hence, this study aimed to investigate the behavior of a series of alkyl-based MOFs by using first principles DFT simulations, thus is to extend current knowledge on pressure-induced structural changes in such structures. First principles DFT calculations have been used to study both the mechanical properties and the behavior of framework materials under pressure, and the results obtained with this method are generally in good agreement with experiments. In these studies, in some cases, DFT calculations have been used to probe deeply into the mechanism behind an experimentally observed phenomenon, while in other cases they have been used as a leading study to reveal a phase transition or anomalous mechanical property that has not yet been observed experimentally. For example, the mechanical properties of ZIF-8 measured by the Brillouin scattering method [37] and its structural flexibility due to the swing effect in imidazole linkers [24,38] have been reproduced with great accuracy by first-principles DFT simulations [23,39,40]. Similarly, it was previously reported experimentally that ZIF-4 exhibits a series of pressure-induced crystalline-crystalline phase transitions prior to amorphization [41], and these phase transitions were then successfully confirmed by first-principles DFT methods [42,43]. However, the negative area compressibility of silver oxalate estimated using first-principles methods [44] has recently been experimentally confirmed [45]. In addition to these studies, there are also materials whose pressure-induced phase transitions and rare piezo-mechanical properties have been reported from first-principles DFT calculations but not yet been experimentally proven [46,47]. Inspired by these works, first, the structural changes of the zinc alky gate framework (ZAG-4) under hydrostatic compression were revisited and confirmed the reliability of our method. Secondly, the high pressure behavior of ZnGA (Zn-Glutarate) and ZnAA (Zn-Adipate) were investigated, suspecting that alkly-carboxylate-based MOFs also exhibit similar flexible behavior. Due to the adaptation of alkyl chains to different conformations in the framework under pressure, it was observed that all structures exhibit outstanding elastic flexibility up to 15 GPa. Even more intriguingly, despite having similar geometries, each of these structures shows different piezo mechanical properties, including very rare phenomena such as zero linear compressibility.

2. Methodology

The periodic DFT calculations were carried out using a plane wave based density functional theory (DFT) as implemented in Quantum Espresso (QE) package [48]. The exchange-correlation functional forms were treated within the framework of generalized gradient approximation (GGA) with Perdew-Burke-Ernzerhof (PBE) parametrization [49]. Electron-ion interactions were described by projector augmented wave (PAW) potential [50]. In order to incorporate van der Waals dispersion interaction, the DFT-D2 method of Grimme was used [51]. Broyden-Fletcher-Goldfarb-Shanno (BFGS) minimization scheme [52] was used for full structural optimization with a convergence criteria of 10^{-3} eV/Å and 10^{-6} eV for residual forces and energy difference between consecutive optimization steps, respectively. A Monkhorst-Pack[53] k-space mesh of $1 \times 3 \times 1$ in reciprocal space was utilized for the Brillouin zone integration. The kinetic energy and charge density cut-off were optimized as 80 and 600 Rydberg, respectively. Using these parameters, the experimentally derived unit cell of ZAG-4 (CCDC 999118), ZnGA (CCDC 166386) and ZnAA (CCDC 825764) were fully relaxed by optimizing both atomic positions and unit cell parameters. Elastic constants of the frameworks were also determined through changes in stress tensor with respect to applied strain using thermo_pw package [54]. The hydrostatic pressure was applied to the framework, and the evolution of unit parameters as a function of pressure was obtained by performing a series of successive enthalpy minimization calculations for each value of pressure starting from the optimized structure. The VESTA [55] program

Table 1
Cell parameters of the MOFs studied in this work compared with experimental and computational studies in the literature. "TW" denotes this study.

MOF	a	b	c	β	V	Space G.	Ref.
ZAG-4(exp)	18.515	8.291	8.265	113.837	1160.5	C2/c (15)	[35]
ZAG-4 (DFT-B3LYP)	18.764	8.440	8.173	112.63	1194.7	C2/c (15)	[19]
ZAG-4 (DFT- GGA-PBE-D2)	18,759	8343	8180	114,022	1169,4	C2/c (15)	TW
ZnGA (exp)	13.934	4.784	9.276	90.628	618.3	P 2/c (13)	[61]
ZnGA (DFT- GGA-PBE-D2)	13.875	4.812	9.387	88.9004	626.6	P 2/c (13)	TW
ZnAA (exp)	16.1050	4.7876	9.2686	90.024	714.65	P 2/c (13)	[62]
ZnAA (DFT-D2 GGA-PBE)	16.25271	4.46704	9.6577	90.4174	701.1445	P 2/c (13)	TW

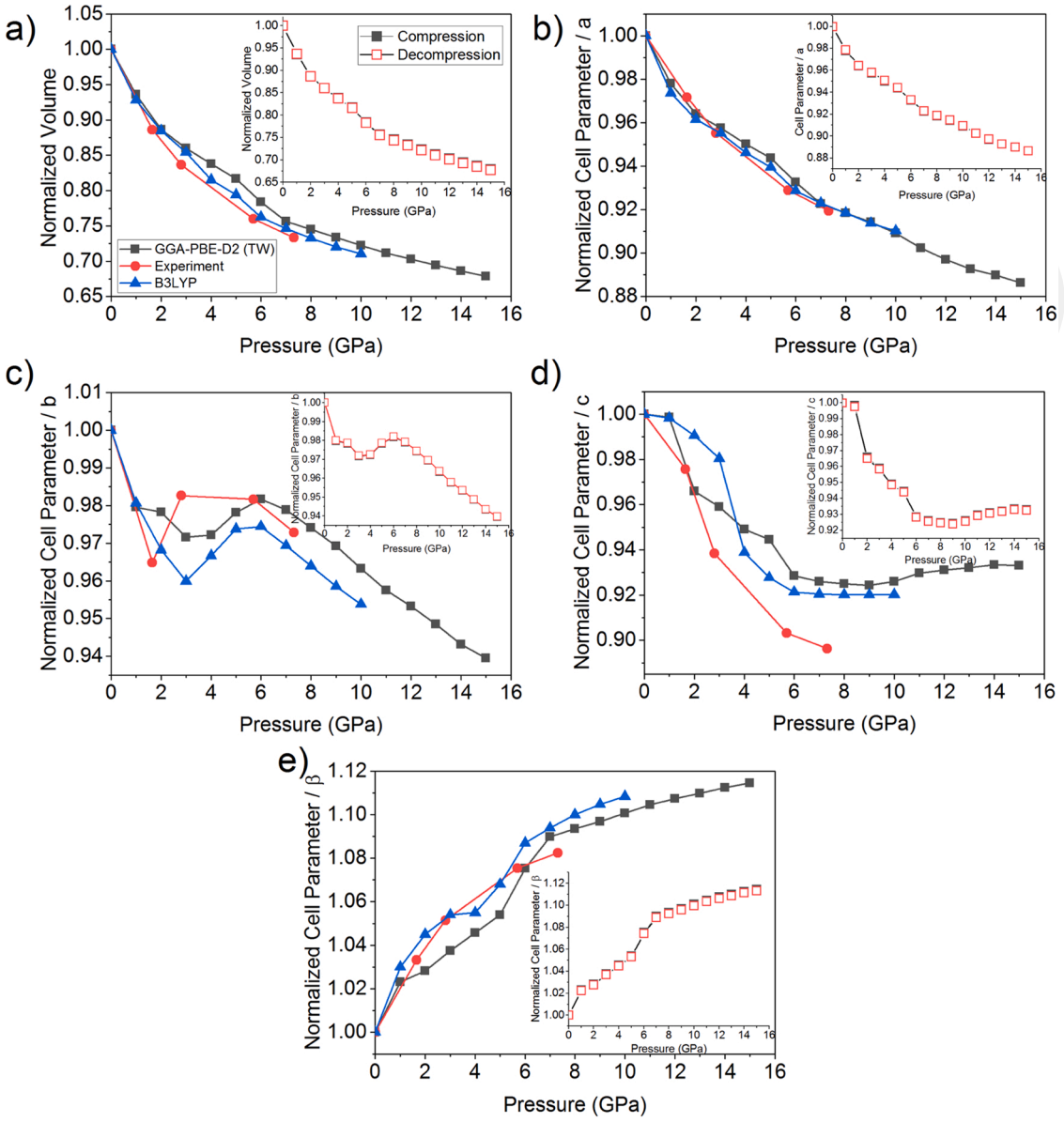

Fig. 2. The evolution of (a) volume and (b-e) lattice parameters of ZAG-4 under hydrostatic compression. TW denotes this work. Experimental and B3LYP simulation values were taken from [35] and [19], respectively.

for visualization, PLATON code [56] for symmetry analysis of high-pressure phases, ELATE [57] and PASCAL [58] codes for derivation of mechanical properties, and ATOMSK [59] for post-processing QE-obtained data were used.

3. Results and discussion

3.1. Zinc alkyl gates (ZAG-4)

ZAG-4 is constructed by bonding two oxygen atoms in each terminal PO_3 group of the alkyl-phosphonate ligand with two different Zn(II) atoms. As a result, formed 8-membered rings ($Zn_2P_2O_4$) are linked through Zn (II) atoms along to c axis to form 1-D inorganic chains. These

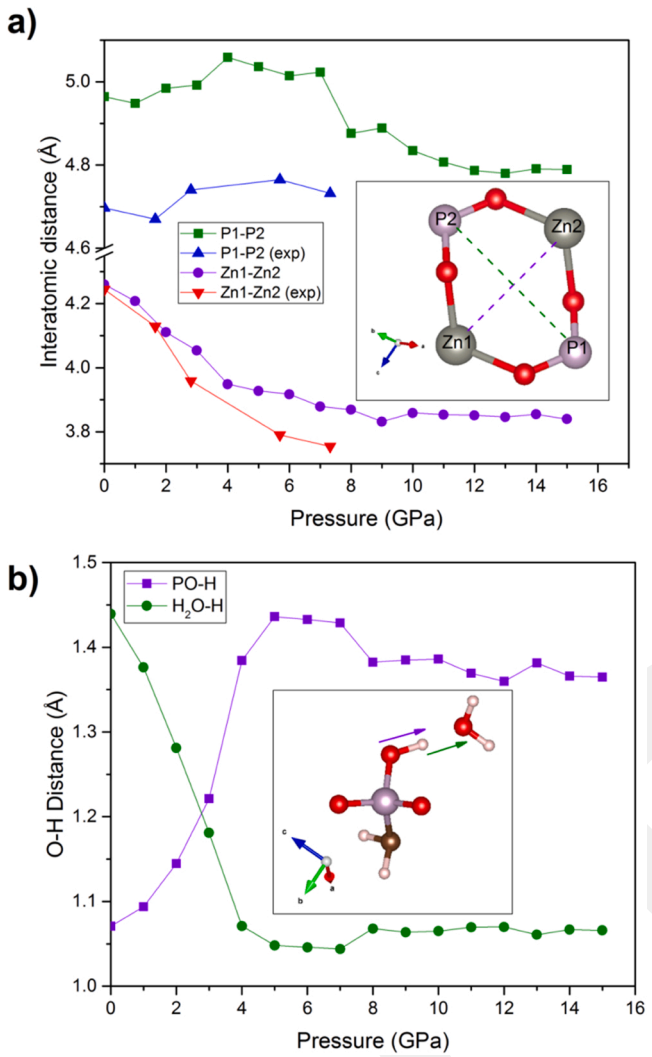

Fig. 3. The origin of the NLC behavior in ZAG-4 is the change in the 8-membered inorganic ring under pressure and the proton transfer between the phosphonate group and the water molecule. a) Pressure-dependent variation of the interatomic distances between Zn-Zn and P-P atoms in 8-membered ring. The inset figure shows the distance between Zn-Zn and P-P atoms in the 8-membered ring. b) Distance of the hopping proton from the oxygen as a function of pressure. The inset figure represents the distances of the proton to the phosphonate and water oxygen.

chains are hydrogen bonded, originated from interstitial water molecules, in one direction to neighboring chains and bridged in the other direction by the butane linker (Fig. 1) [35,60]. The framework has monoclinic symmetry, space group C2/c (15). The calculated cell parameters are summarized in Table 1. All cell parameters of the ZAG-4 is consistent (within ± 1%) with available experimental and DFT data. The hydrostatic pressure dependence of volumes and unit cells parameters for both structures is presented in Fig. 2. Clearly, the evolution of the cell parameters and volume under compression satisfactorily concurs with the previous findings [19,35]. The volume decreases 25% up to 7 GPa. However, in the higher pressure range, the frameworks are less responsive to the applied pressure, with further a volume change of only 7% between 7 and 15 GPa. Despite the about 32% reduction in volume and the drastic change in cell parameters, frameworks restore to initial configuration within reasonable calculation error by the removal of pressure (Fig. 2a). As well, there is no onset of amorphization or structural failure for ZAG-4 over the pressure range studied. Evidently, the a parameter is monotonically shrinking in the pressure region studied (Fig. 2b). On the other hand, as already reported, the b parameter first compresses and then elongates in a non-monotonically behavior (Fig. 1c). Correlatively, a sudden drop in the c parameter is observed in the same pressure range (Fig. 1d). The monoclinic β angle shows a significant increase in the pressure region studied (Fig. 1e).

The origin of the negative linear compressibility (NLC) observed at high pressures in the b-axis is interconnected with the change in 1-D inorganic chains and pressure-induced proton transfer. Fig. 3a shows the pressure-dependent evolution of the interatomic distance between atoms in the 8-membered ring. The distortion of the ring is a result of an opening in the O1-Zn1-O2 angle, leading to a decrease in Zn1-Zn1 distance from 4.26 to 3.84 Å. Simultaneously, on the other hand, the distance between P1-P2 increases from 4.96 to 5.06 between 0 and 4 GPa and then reduces to 4.79 at 15 GPa. The most interesting feature of the framework is the pressure-induced proton transfer from the phosphonate group to the water molecule. This piezo-mechanical response is characterized by the change of the O-H distance between the proton and the oxygen atoms of the phosphonate group and the water molecule (Fig. 3b). Under compression, since the -PO_3H group of the ligand is closer to the water molecule, in the range of 3–4 GPa, the proton jumps to the water molecule and forms the H_3O^+ ion. At higher compression values, no other structural transition is observed, although there are fluctuations in the O-H distance due to the dynamic structure and hydrogen bonding. However, when the pressure is removed, the proton jumps back to the phosphonate group, indicating that ZAG-4 is a promising material for various sensor and actuator applications.

3.2. *Zinc alkyl dicarboxylates: (ZADs)*

In order to investigate the structural flexibility of alky dicarboxylate based MOF, ZnGa (Zinc Glutarate) and ZnAA (Zinc Adipate) were used as the proof-of-concept prototypical frameworks. These frameworks have the same monoclinic symmetry with space group P2/c and a very similar structure. In the frameworks, Zn atoms are tetrahedrally coordinated by four carboxyl O atoms of different alkyl-carboxylate ligands which bis-bidentately link four Zn atoms a 3-D network (Fig. 1). The linkers connect the tetrahedral groups along the a-axis; hence only unit cell parameter "*a*" differs considerably in each structure depending on the length of C-backbone of the alkyl-carboxylate linker. The relaxed cell parameters of both structures are listed in Table 1. They are in good agreement with experimental values.

In ZnGa, the glutarate ligand has either a bent (type-1) or fully extended (type-2) conformation (Figs. 4a and c). These ligands, coordinated with four different Zn(II) ions, form two types of rings in the framework. The 16-membered ring (16-MR) is formed by coordination of two Zn(II) ions and two glutarate ligands with type-1 conformation. The 24-membered ring (24-MR) consists of 4 Zn(II) ions and two glutarate ligands in type-2 and two carboxyl groups on two glutarate in type-2 conformations (Fig. 4b) [61].

The pressure dependence unit cell parameters and volume of ZnGA is shown in Fig. 5a. Obviously, the cell volume gradually decreases with the increases of the pressure. When the pressure reaches 15 GPa, the volume decreases by 27%, with the largest change of 14% occurring in the first 4 GPa. All lattice constants show positive linear compressibility and shrink equally by about 10% at 15 GPa. ZnGa, like ZAG-4, returns to its relaxed configuration when pressure is removed, implying structural elasticity of the framework up to 15 GPa. The framework doesn't exhibit any phase transition or amorphization onset within the applied hydrostatic compression investigated. All metastable structures obtained in this compression region have P2/c symmetry and the glutarate ligands adopt the (1111) coordination mode [28] in all structures.

To provide complete explanation for the behavior of ZnGa under a hydrostatic compression, the evolution of 16-MR, 24-MR, Zn-O bonds and O-Zn-O bond angles were investigated. The longest interatomic distance of 16-MR is defined by distance between two Zn atoms, while it is given by the interatomic distance between two O atoms for the 24-MR. The largest distortions are located in 16-MR containing only type-1

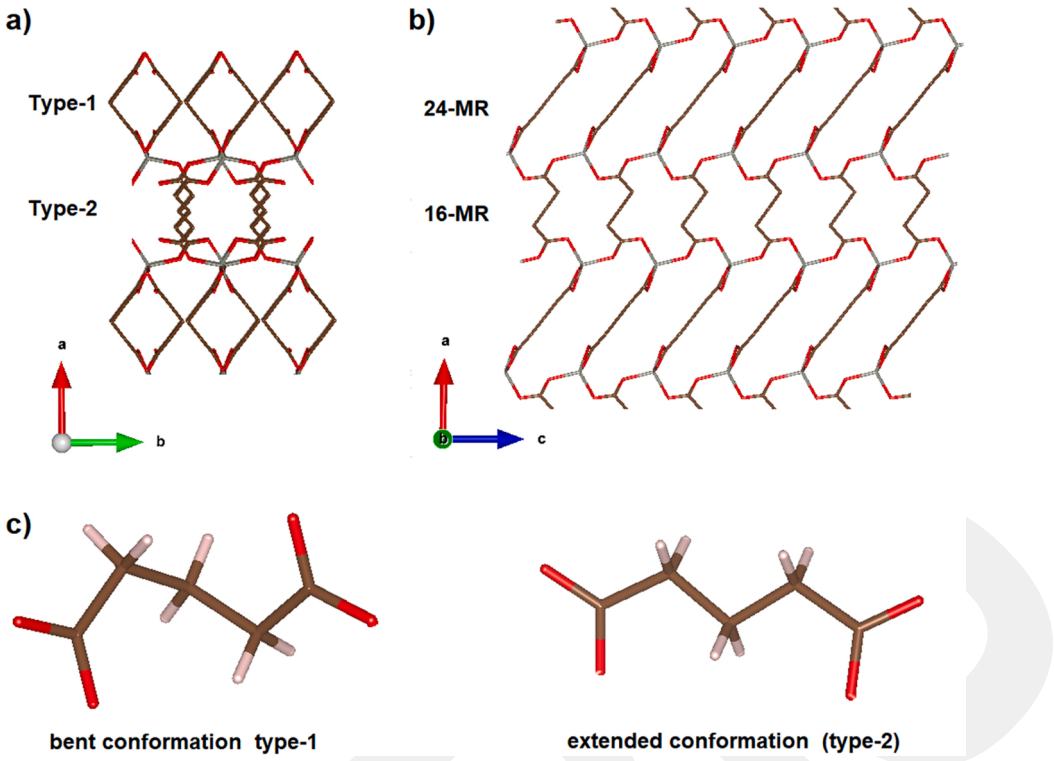

Fig. 4. Molecular network structure of ZnGA. View down (a) the c-axis and (b) the b-axis showing 16- and 24-membered rings formed by the coordination of glutarate ligands to Zn-II ions in two different conformations. (c) Bent and extended conformations of glutarate ligands.

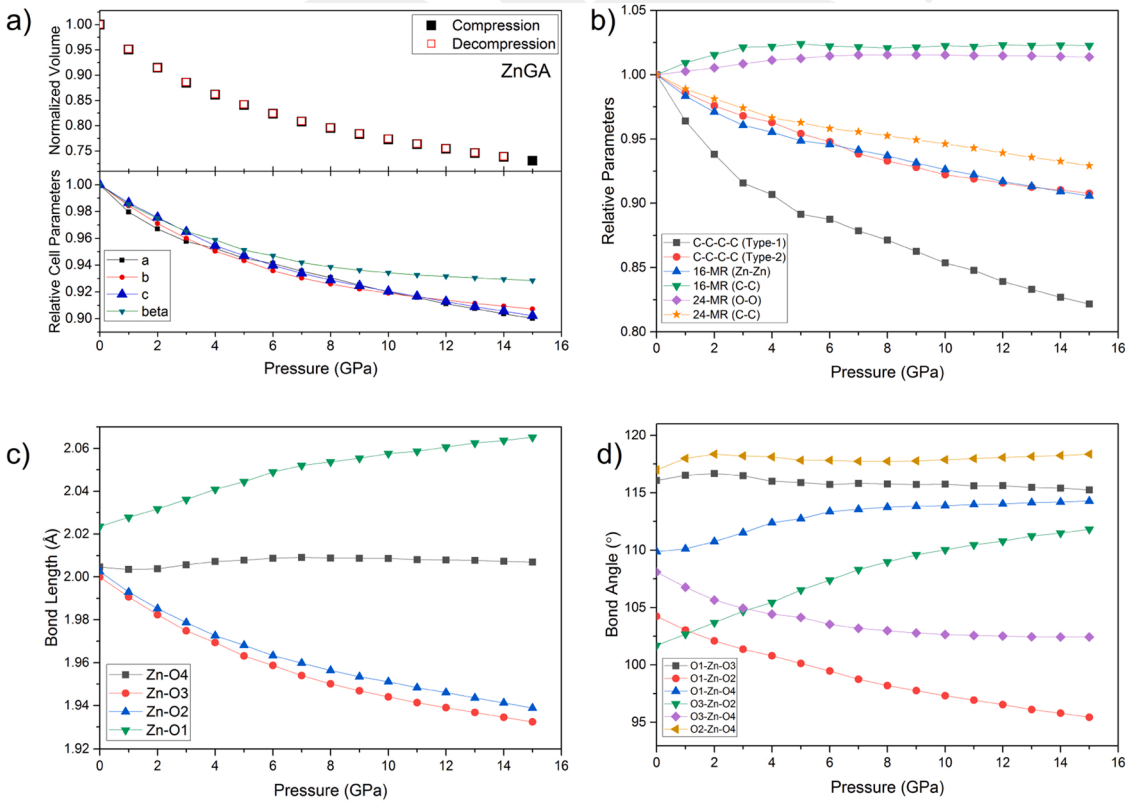

Fig. 5. Evolution of (a) unit cell volume and parameters, (b) 16-MR and 24-MR, (c) bond lengths, and (d) bond angles in ZnGA as a function of pressure.

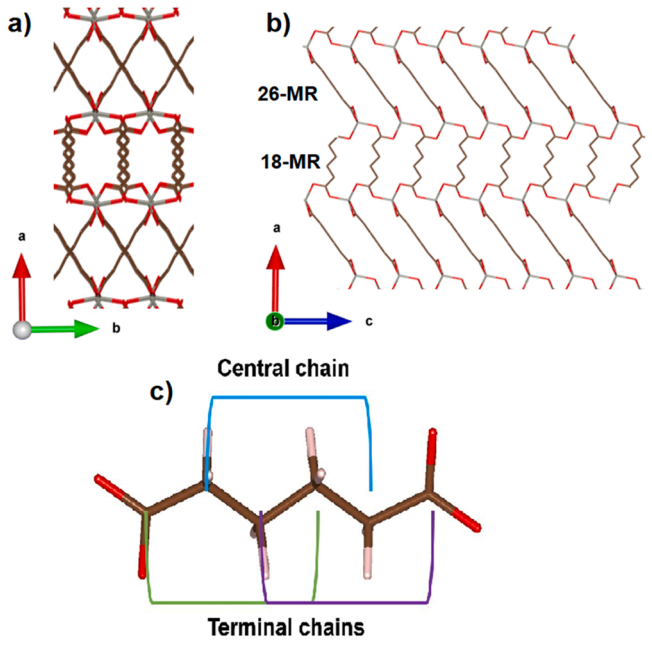

Fig. 6. Molecular network structure of ZnAA. View down (a) the c-axis and (b) the b-axis showing 18- and 26-membered rings formed by the coordination of adipate ligands to Zn-II ions in a nearly extended conformation. (c) Molecular structure of the adipate ligand.

glutarate. Accordingly, while the Zn-Zn distance in the ring decreases from 7.08 Å to 6.41 Å, the interatomic distance between the C-C atoms that define the width of the ring increases from 6.50 Å to 6.65 A (Fig. 5b). Normally, such a compression in the ring is expected to be the result of an expansion in the O1-Zn-O2 angle, but both the compression due to the flexible nature of the type-1 ligand and the mutual coordination between the two rings cause a narrowing in the O1-Zn-O2 angle (Fig. 1d). However, relatively less deformation is observed in 24-MR because of less compression of type-2 glutarate. So, while the distance between O-O increases from 12.74 Å to 12.92 Å, the distance between C-C decreases from 4.73 Å to 4.40 Å (Fig. 5b). The lengths of the type-1 ligand and type-2 ligands are shortened by 13.3% and 3.3%, respectively, compared to the relaxed value at 15 GPa. Both this and the change in the Zn-O tetrahedral angles and Zn-O bond lengths in the ring further confirm that 16-MR undergoes more deformation (Fig. 5c-d).

ZnAA has the same structural motifs as ZnGa. The metal-rings have 18 and 26 members due the longer alkyl chain of the ligand extend in the ac plane, and make infinitely eclipsed stacks along to the b axis (Fig. 6a-b). However, although adipate ligands conform to the (1111) coordination mode, which denotes that each of the four oxygen atoms of the adipate unit is coordinated to only one Zn atom [28], 16-MRs and 24-MRs are formed by ligands with a nearly extended conformation (Fig. 6c) (Figure SX). The ligands forming 16MR, therefore, show 2-fold interpenetration along the crystallographic b-axis [62].

The behavior of ZnAA under pressure is shown in Fig. 7a. The volume of the framework is continuously decreasing under pressure. Already, the structure shrinks by 24% compared to the initial volume at 15 GPa. However, unlike ZnGa, the lattice parameters do not change monotonously with pressure. At 15 GPa, lattice parameters b and c shrink by 13.5% and 7.5%, respectively. However, the compression at a is only around 5%, and interestingly, no appreciable change is observed up to 5 GPa.

In the optimized structure, the terminal chains for type-1 and type-2 adipates have a nearly extended conformation (torsion angles 177 and 175, respectively), while the main chains have a perfectly extended conformation. The central chains of ligands maintain their perfectly extended conformation throughout the applied pressure regime (Fig. 7b). However, the terminal carbon chains, including the carboxylate carbon in coordination with Zn-O, considerably deform under

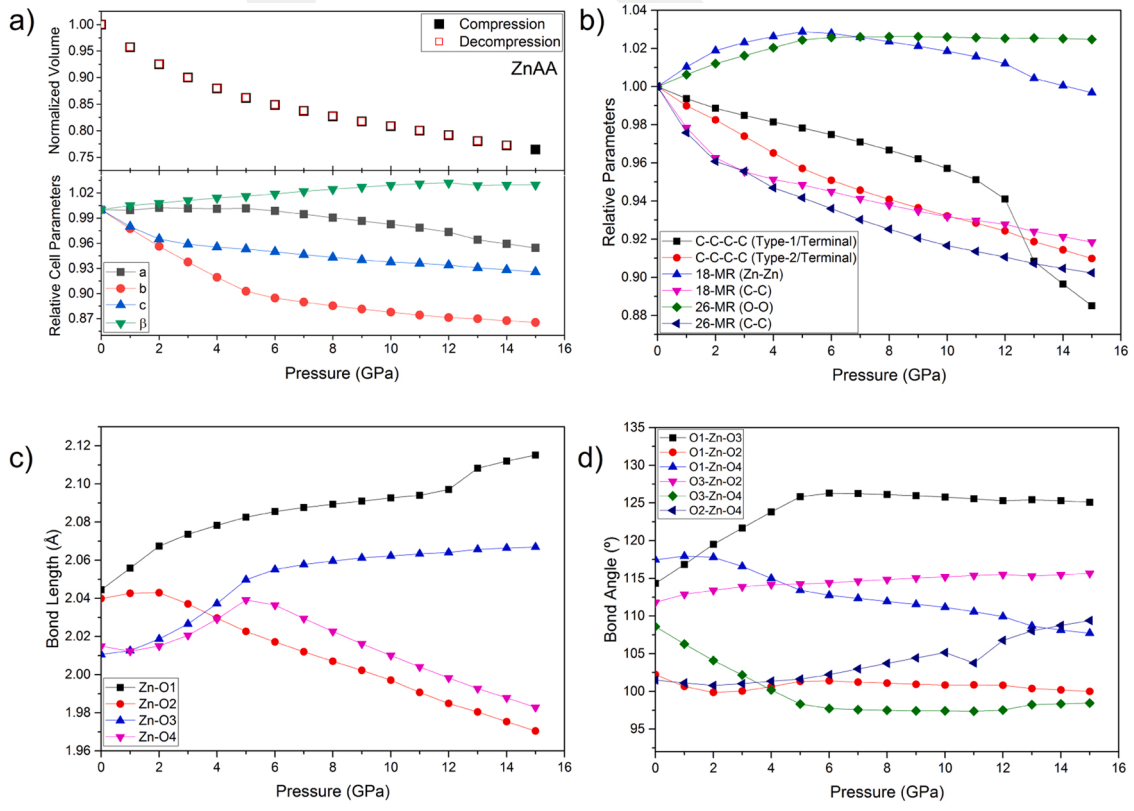

Fig. 7. Evolution of (a) unit cell volume and parameters, (b) 18-MR and 26-MR, (c) bond lengths, and (d) bond angles as a function of pressure.

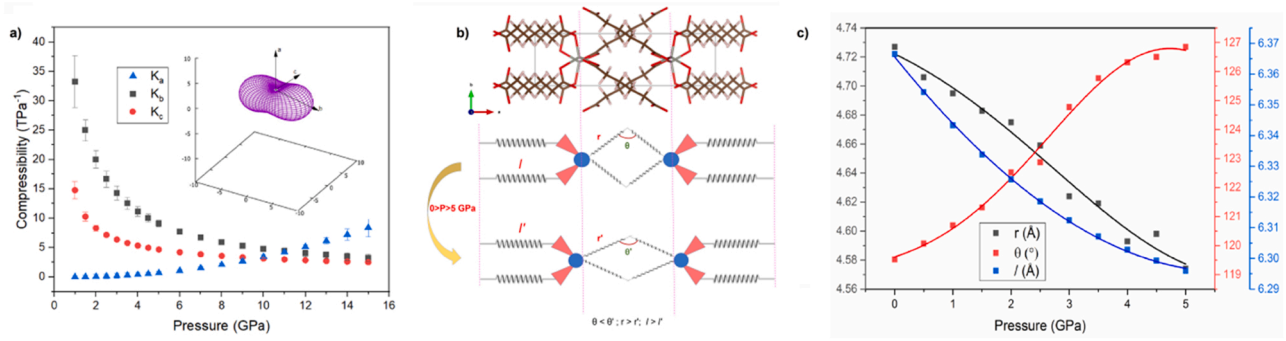

Fig. 8. (a) The linear compressibility of the unit cell of ZnAA. (b) Structure of ZnAA in the xy plane under ambient conditions and schematic representation of the structure. The springs, blue circles and red triangles correspond to alkyl chains, Zn(II) ion and carboxylate oxygens, respectively. The evolution of the proposed structural motif at ambient conditions (middle) and at high pressure (bottom) is shown.(c) Competitive evolution of r (strut length), θ (hinge angle) and *l*(alkyl chain length) under pressure.

pressure (Fig. 7c). At 15 GPa, the terminal dihedral angles of type-1 and type-2 ligands decrease to 156° and 159° due to compression in the structure (Fig. 7d). In this region, the lengths of the type-1 and type-2 adipates are shortened by approximately 4% and 2%, respectively. The more compression of the structure along the b and c axes causes more shortening of the Zn-O bond lengths in these directions. For example, the Zn-O4 bond length along the b axis decreases from 2.015 A to 1.982 A in the studied pressure range (Fig. 7c). Zn-O tetrahedra also significantly deform under compression, however, the bond angles show different trends due to mechanical anisotropy (Fig. 7d).

As mentioned above, the most striking feature of ZnAA is its zero linear compressibility (ZLC) along the a-axis. ZLC is when a material neither stretches nor shortens along an axis under hydrostatic pressure, contrary to expectations [63]. By convention, linear compressibility with an absolute value lower than that of the diamond (0.75 TPa^{-1}) is defined as ZLC [64]. Between 0 and 5 GPa, ZnAA shows a very small negative linear compressibility (−0.22 TPa^{-1}), which, by definition, indicates that ZnAA exhibits ZLC (Fig. 8a). From a design point of view, a material with ZLC can be produced as a composite of two materials showing NLC and PLC. It is also a rational option to design a single-phase material that exhibits both NLC and PLC along the same axis [65]. The rhombus geometries in the xy-plane of ZnAA create a specific motif that is responsible for the negative linear compressibility (NLC). These rhombus geometries are connected via Zn(II) ions to horizontal spring-like alkyl chains that exhibit positive linear compressibility (PLC). Under compression - as in MOFs exhibiting NLC - the strut length in the rhombus geometry shortens while the hinge angle increases (Fig. 8b). The larger increase in the hinge angle leads to elongation along the a-axis ($d=rsin\theta$). This elongation is transferred through Zn(II) to the alkyne chains, causing a shortening of the chains. The competitive effect between these two structural geometries causes the a-axis to remain stable up to a specific compression limit. This mechanism is very similar to the dumbbell-like model reported by Li et al. [65]. The r, theta, and adipate length plotted as a function of pressure in Fig. 8c confirm this hypothesis. Above 5 GPA, the structure shows PLC along the a-axis as the dominance of C-H···O hydrogen bonds between methylene hydrogens and carboxylate oxygens under compression disrupts the rhombus geometry.

Obviously, both ZnGA and ZnAA show outstanding elastic flexibility. This behavior was experimentally demonstrated in the study, which proved that ZnGA and ZnAA retain their crystallinity even after a 4-hour ball milling process, although it does not correspond to a hydrostatic compression process [62]. Unlike the pressure-induced bond breakage reported for UiO-66 [66] or the amorphization seen in ZIF-8 [40,67] and MOF-5 [68], alkyl chains with spring-like behavior allow large deformations in the structures, thus stabilizing the structures by preserving the metal-ligand coordination. The closing of methylene groups to carboxylate oxygens under compression causes weak C-H···O hydrogen bonds between these two species. C-H···O bonds, which play an important role in the structural stabilization of biological macromolecules, may be responsible for the elastic flexibility of ZnGa and ZnAA and the fact that the structures are stabilized beyond 6 GPa and less responsive to pressure [69–71]. The longer alky chain causes domination of the C-H···O hydrogen bonds at lower compression. Hence, the relatively less deformation of ZnAA compared to ZnGA can be attributed to this phenomenon. As well, steric congestion due to pressure-induced volume reduction could well be responsible for the fewer structural changes in the framework [72,73].

Elastic constants reflect the resistance of a crystal to externally applied pressure, as well as provide information about the thermal and acoustic properties of solids. Due to the lower symmetry of the monoclinic structure, there are 13 independent elastic constants (C_{ij}): C_{11}, C_{22} and C_{33} are the principal elastic constants; C_{44}, C_{55} and C_{66} are the shear elastic constants; C_{12}, C_{23}, C_{15}, C_{25}, C_{35} and C_{46} are the seven off-diagonal elastic constants. Elastic constants of all 3 frameworks are listed in Table 2. Accordingly, all three structures are mechanically stable since they meet the Born-Huang stability criteria for monoclinic crystals [74]:

$$C_{11} > 0, C_{22} > 0, C_{33} > 0, C_{44} > 0, C_{55} > 0, C_{66} > 0$$
$$C_{44}C_{66} - 2C_{46} > 0$$
$$C_{11} + C_{22} + C_{33} + 2(C_{12} + C_{13} + C_{23}) > 0$$
$$C_{22} + C_{33} - 2C_{23} > 0$$

In order to analyze the elastic tensors of the frameworks, ELATE [57] was used. The calculated bulk moduli for ZAG-4, ZnGA and ZnAA are 14.77, 16.85 and 21.19 GPa, respectively, which ranks somewhere between rigid and breathing MOFs [19]. The relatively low bulk compressibility of ZnAA is in agreement with the P-V values obtained from the geometry optimization results. Although the elastic constants we found for ZAG-4 are slightly different from those reported [19]

Table 2
The calculated independent elastic constant of MOFs (in GPa).

MOF	C_{11}	C_{22}	C_{33}	C_{44}	C_{55}	C_{66}	C_{12}	C_{13}	C_{15}	C_{23}	C_{25}	C_{35}	C_{46}
ZAG-4	25.33	21.30	36.41	14.63	25.30	2.07	10.63	20.39	-18.93	15.13	-4.81	-12.01	-1.71
ZnGA	37.92	41.79	24.60	3.84	17.92	8.66	10.64	18.97	11.82	4.11	5.11	7.07	4.48
ZnAA	42.48	39.45	23.09	4.40	11.50	17.09	17.35	18.30	-6.58	7.20	-2.80	-4.17	-8.15

previously, the mechanical properties derived from them are in good agreement with that study. For example, ZAG-4 shows a modest NLC (-18.57 TPa^{-1}) in the elastic region as reported by Coudert et al. [19]. ZnGA, with all elastic constants positive, shows only PLC in all directions. ZnAA, as expected, shows a very small NLC (-0.52 TPa^{-1}) along the a-axis, which corresponds to ZLC by definition. For all structures, the direction-dependent variations of the mechanical properties are given in the supporting information, implying that the lattice structures show high mechanical anisotropy.

4. Conclusions

In conclusion, first-principles DFT simulations were used to study the behavior of Zn-alkyl-based MOFs under pressure and to determine their mechanical properties. Due to the lack of experimental data for ZnGA and ZnAA, the reliability of the simulation parameters was tested by taking ZAG-4, whose structural flexibility has been previously reported experimentally and computationally, as a benchmark. Evidently, PBE-PAW with Grimme's dispersion correction is capable of simulating the behavior of flexible MOFs under pressure with great accuracy. On the other hand, it should be noted that the effect of thermal fluctuations is neglected due to the fact that the calculations in this study are performed at zero Kelvin and the effects of surface and structure defects are ignored due to periodic boundary conditions. Although these limitations, which arise from the inherent formalism of first-principles DFT calculations, to some extent, lead to over/underestimation of critical values, they are negligible when the correct calculation parameters are chosen. All three structures were observed to undergo elastic deformation under hydrostatic compression up to 15 GPa, as the alkyl chains allow the structure to move without disrupting the metal-ligand coordination. Notably, despite their similar crystal structure and ligands, the three structures exhibited distinct piezomechanical properties, namely NLC, PLC, and ZLC for ZAG-4, ZnGA, and ZnAA, respectively. The NLC observed in ZAG-4 is due to the proton transfer between the phosphonate oxygen and the water in the structure, while the ZLC in ZnAA is due to the dumbbell-like structural motif formed by the substructures showing NLC and PLC. Therefore, owing to the tailorable structures of MOFs, it is possible to synthesize frameworks with high flexibility and anomalous mechanical properties with a rational design. In this context, the presented findings may inspire the synthesis of such materials.

CRediT authorship contribution statement

Mustafa Erkartal: Conceptualization, Investigation, Methodology, Resources, Software, Visualization, Writing – review & editing.

Declaration of Competing Interest

The authors declare that they have no known competing financial interests or personal relationships that could have appeared to influence the work reported in this paper.

Data availability

The data that support the findings of this study are available on request from the corresponding author.

Acknowledgements

The calculations were run on The Scientific and Technological Research Council of Turkey (TÜBİTAK) ULAKBILIM, High Performance and Grid Computing Center (TRUBA) and AGU-HPC resources.

Appendix A. Supporting information

Supplementary data associated with this article can be found in the online version at doi:10.1016/j.mtcomm.2023.106054.

References

[1] H. Furukawa, K.E. Cordova, M. O'Keeffe, O.M. Yaghi, The chemistry and applications of metal-organic frameworks, Science 341 (6149) (2013) 974.
[2] Y. Guclu, H. Erer, H. Demiral, C. Altintas, S. Keskin, N. Tumanov, B.L. Su, F. Semerci, Oxalamide-functionalized metal organic frameworks for CO_2 adsorption, Acs Appl. Mater. Inter 13 (28) (2021) 33188–33198.
[3] M. Tabatabaii, M. Khajeh, A.R. Oveisi, M. Erkartal, U. Sen, Poly(lauryl methacrylate)-Grafted Amino-Functionalized Zirconium-Terephthalate Metal-Organic Framework: Efficient Adsorbent for Extraction of Polycyclic Aromatic Hydrocarbons from Water Samples, Acs Omega 5 (21) (2020) 12202–12209.
[4] S.H. Yang, A.J. Ramirez-Cuesta, R. Newby, V. Garcia-Sakai, P. Manuel, S.K. Callear, S.I. Campbell, C.C. Tang, M. Schroder, Supramolecular binding and separation of hydrocarbons within a functionalized porous metal-organic framework, Nat. Chem. 7 (2) (2015) 121–129.
[5] W. Gong, Y. Xie, X.J. Wang, K.O. Kirlikovali, K.B. Idrees, F.R. Sha, H.M. Xie, Y. Liu, B.L. Chen, Y. Cui, O.K. Farha, Programmed Polarizability Engineering in a Cyclen-Based Cubic Zr(IV) Metal-Organic Framework to Boost Xe/Kr Separation, J. Am. Chem. Soc. (2023).
[6] K.E. McCullough, D.S. King, S.P. Chheda, M.S. Ferrandon, T.A. Goetjen, Z.H. Syed, T.R. Graham, N.M. Washton, O.K. Farha, L. Gagliardi, M. Delferro, High-Throughput Experimentation, Theoretical Modeling, and Human Intuition: Lessons Learned in Metal–Organic-Framework-Supported Catalyst Design, Acs Cent. Sci. 9 (2) (2023) 266–276.
[7] W.J. Shen, Ionic exchange of metal-organic frameworks to access single nickel sites for efficient electroreduction of CO_2, Acta Phys. -Chim. Sin. 34 (2) (2018) 113–114.
[8] Q.L. Zhu, J. Li, Q. Xu, Immobilizing metal nanoparticles to metal-organic frameworks with size and location control for optimizing catalytic performance, J. Am. Chem. Soc. 135 (28) (2013) 10210–10213.
[9] U. Sen, M. Erkartal, C.W. Kung, V. Ramani, J.T. Hupp, O.K. Farha, Proton conducting self-assembled metal-organic framework/polyelectrolyte hollow hybrid nanostructures, Acs Appl. Mater. Inter 8 (35) (2016) 23015–23021.
[10] S.N. Zheng, D.L. Sun, L.L. Wu, S.M. Liu, G.H. Liu, Carbon fiber supported two-dimensional ZIF-7 interlayer for durable lithium-sulfur battery, J. Alloy. Compd. 870 (2021).
[11] C.W. Gao, Z.J. Jiang, S.B. Qi, P.X. Wang, L.R. Jensen, M. Johansen, C. K. Christensen, Y.F. Zhang, D.B. Ravnsbaek, Y.Z. Yue, Metal-organic framework glass anode with an exceptional cycling-induced capacity enhancement for lithium-ion batteries, Adv. Mater. 34 (10) (2022).
[12] S. Mukhopadhyay, A. Das, T. Jana, S.K. Das, Fabricating a MOF material with polybenzimidazole into an efficient proton exchange membrane, Acs Appl. Energ. Mater. 3 (8) (2020) 7964–7977.
[13] C. Li, T.T. Zhang, J.Y. Zhao, H. Liu, B. Zheng, Y. Gu, X.Y. Yan, Y.R. Li, N.N. Lu, Z. Q. Zhang, G.D. Feng, Boosted sensor performance by surface modification of bifunctional rht-type metal-organic framework with nanosized electrochemically reduced graphene oxide, Acs Appl. Mater. Inter 9 (3) (2017) 2984–2994.
[14] J.H. Dou, M. Dinca, Signature of metallic behavior in the metal-organic frameworks M3(hexaiminobenzene)2 (M = Ni, Cu), Abstr. Pap. Am. Chem. S 255 (2018).
[15] J.G. Park, M.L. Aubrey, J. Oktawiec, K. Chakarawet, L.E. Darago, F. Grandjean, G. J. Long, J.R. Long, Charge delocalization and bulk electronic conductivity in the mixed-valence metal-organic framework Fe(1,2,3-triazolate)(2)(BF4)(x), J. Am. Chem. Soc. 140 (27) (2018) 8526–8534.
[16] Y.Z. Xing, L.X. Shi, J. Yan, Y.L. Chen, High-performance methanal sensor based on metal-organic framework based one-dimensional photonic crystal, Chemistryselect 5 (13) (2020) 3946–3952.
[17] J. Perego, C.X. Bezuidenhout, I. Villa, F. Cova, R. Crapanzano, I. Frank, F. Pagano, N. Kratochwill, E. Auffray, S. Bracco, A. Vedda, C. Dujardin, P.E. Sozzani, F. Meinardi, A. Comotti, Highly luminescent scintillating hetero-ligand MOF nanocrystals with engineered Stokes shift for photonic applications, Nature, Communications 13 (1) (2022).
[18] P. Tholen, C.A. Peeples, M.M. Ayhan, L. Wagner, H. Thomas, P. Imbrasas, Y. Zorlu, C. Baretzky, S. Reineke, G. Hanna, G. Yucesan, Tuning structural and optical properties of porphyrin-based hydrogen-bonded organic frameworks by metal insertion, Small 18 (49) (2022).
[19] A.U. Ortiz, A. Boutin, K.J. Gagnon, A. Clearfield, F.X. Coudert, Remarkable pressure responses of metal-organic frameworks: proton transfer and linker coiling in zinc alkyl gates, J. Am. Chem. Soc. 136 (32) (2014) 11540–11545.
[20] J.F. Lyu, X.Y. Gong, S.J. Lee, K. Gnanasekaran, X. Zhang, M.C. Wasson, X.J. Wang, P. Bai, X.H. Guo, N.C. Gianneschi, O.K. Farha, Phase Transitions in Metal-Organic Frameworks Directly Monitored through In Situ Variable Temperature Liquid-Cell Transmission Electron Microscopy and In Situ X-ray Diffraction, J. Am. Chem. Soc. 142 (10) (2020) 4609–4615.
[21] G.F. Turner, S.C. McKellar, D.R. Allan, A.K. Cheetham, S. Henke, S.A. Moggach, Guest-mediated phase transitions in a flexible pillared-layered metal-organic framework under high-pressure, Chem. Sci. 12 (41) (2021) 13793–13801.
[22] D.M. Polyukhov, S. Krause, V. Bon, A.S. Poryvaev, S. Kaskel, M.V. Fedin, Structural Transitions of the Metal-Organic Framework DUT-49(Cu) upon Physi- and Chemisorption Studied by in Situ Electron Paramagnetic Resonance Spectroscopy, J. Phys. Chem. Lett. 11 (15) (2020) 5856–5862.
[23] F.X. Coudert, Molecular mechanism of swing effect in zeolitic imidazolate framework ZIF-8: continuous deformation upon adsorption, Chemphyschem 18 (19) (2017) 2732–2738.

[24] C.L. Hobday, T.D. Bennett, D. Fairen-Jimenez, A.J. Graham, C.A. Morrison, D. R. Allan, T. Duren, S.A. Moggach, Tuning the Swing Effect by Chemical Functionalization of Zeolitic Imidazolate Frameworks, J. Am. Chem. Soc. 140 (1) (2018) 382–387.
[25] C. Serre, F. Millange, C. Thouvenot, M. Nogues, G. Marsolier, D. Louer, G. Ferey, Very large breathing effect in the first nanoporous chromium(III)-based solids: MIL-53 or Cr-III(OH)center dot{O2C-C6H4-CO_2}center dot{HO2C-C6H4-CO_2H}(x) center dot H2Oy, J. Am. Chem. Soc. 124 (45) (2002) 13519–13526.
[26] J. Tang, Y.Y. Chu, S.H. Li, J. Xu, W.P. Xiong, Q. Wang, F. Deng, Breathing Effect via Solvent Inclusions on the Linker Rotational Dynamics of Functionalized MIL-53, Chem. -Eur. J. 27 (59) (2021) 14711–14720.
[27] S. Krause, V. Bon, I. Senkovska, U. Stoeck, D. Wallacher, D.M. Tobbens, S. Zander, R.S. Pillai, G. Maurin, F.X. Coudert, S. Kaskel, A pressure-amplifying framework material with negative gas adsorption transitions, Nature 532 (7599) (2016) 348–352.
[28] T.K. Kim, K.J. Lee, M. Choi, N. Park, D. Moon, H.R. Moon, Metal-organic frameworks constructed from flexible ditopic ligands: conformational diversity of an aliphatic ligand, N. J. Chem. 37 (12) (2013) 4130–4139.
[29] T.T.Y. Tan, X. Li, K. Otake, Y.C. Tan, X.J. Loh, S. Kitagawa, J.Y.C. Lim, UiO-66 metal organic frameworks with high contents of flexible adipic acid co-linkers, Chem. Commun. 58 (81) (2022) 11402–11405.
[30] P.M. Forster, A.R. Burbank, C. Livage, G. Ferey, A.K. Cheetham, The role of temperature in the synthesis of hybrid inorganic-organic materials: the example of cobalt succinates, Chem. Commun. 4 (2004) 368–369.
[31] H. Reinsch, I. Stassen, B. Bueken, A. Lieb, R. Ameloot, D. De Vos, First examples of aliphatic zirconium MOFs and the influence of inorganic anions on their crystal structures, Crystengcomm 17 (2) (2015) 331–337.
[32] H. Reinsch, R.S. Pillai, R. Siegel, J. Senker, A. Lieb, G. Maurin, N. Stock, Structure and properties of Al-MIL-53-ADP, a breathing MOF based on the aliphatic linker molecule adipic acid, Dalton Trans. 45 (10) (2016) 4179–4186.
[33] G. Alberti, S. Murcia-Mascaros, R. Vivani, Pillared derivatives of gamma-zirconium phosphate containing nonrigid alkyl chain pillars, J. Am. Chem. Soc. 120 (36) (1998) 9291–9295.
[34] C.X. Bezuidenhout, V.J. Smith, C. Esterhuysen, L.J. Barbour, Solvent- and Pressure-Induced Phase Changes in Two 3D Copper Glutarate-Based Metal-Organic Frameworks via Glutarate (plus gauche reversible arrow -gauche) Conformational Isomerism, J. Am. Chem. Soc. 139 (16) (2017) 5923–5929.
[35] K.J. Gagnon, C.M. Beavers, A. Clearfield, MOFs under pressure: the reversible compression of a single crystal, J. Am. Chem. Soc. 135 (4) (2013) 1252–1255.
[36] S.J. Wang, N. Xhaferaj, M. Wahiduzzaman, K. Oyekan, X. Li, K. Wei, B. Zheng, A. Tissot, J. Marrot, W. Shepard, C. Martineau-Corcos, Y. Filinchuk, K. Tan, G. Maurin, C. Serre, Engineering structural dynamics of zirconium metal organic frameworks based on natural C4 linkers, J. Am. Chem. Soc. 141 (43) (2019) 17207–17216.
[37] J.C. Tan, B. Civalleri, C.C. Lin, L. Valenzano, R. Galvelis, P.F. Chen, T.D. Bennett, C. Mellot-Draznieks, C.M. Zicovich-Wilson, A.K. Cheetham, Exceptionally low shear modulus in a prototypical imidazole-based metal-organic framework, Phys. Rev. Lett. 108 (9) (2012).
[38] M.E. Casco, Y.Q. Cheng, L.L. Daemen, D. Fairen-Jimenez, E.V. Ramos-Fernandez, A.J. Ramirez-Cuesta, J. Silvestre-Albero, Gate-opening effect in ZIF-8: the first experimental proof using inelastic neutron scattering, Chem. Commun. 52 (18) (2016) 3639–3642.
[39] W. Zhang, J. Maul, D. Vulpe, P.Z. Moghadam, D. Fairen-Jimenez, D.M. Mittleman, J.A. Zeitler, A. Erba, M.T. Ruggiero, Probing the mechanochemistry of metal-organic frameworks with low-frequency vibrational spectroscopy, J. Phys. Chem. C. 122 (48) (2018) 27442–27450.
[40] M. Erkartal, M. Durandurdu, Pressure-induced amorphization, mechanical and electronic properties of zeolitic imidazolate framework (ZIF-8), Mater. Chem. Phys. 240 (2020).
[41] S. Henke, M.T. Wharmby, G. Kieslich, I. Hante, A. Schneemann, Y. Wu, D. Daisenberger, A.K. Cheetham, Pore closure in zeolitic imidazolate frameworks under mechanical pressure, Chem. Sci. 9 (6) (2018) 1654–1660.
[42] Z.H. Shi, K.Y. Weng, N. Li, The Atomic Structure and Mechanical Properties of ZIF-4 under High Pressure: Ab Initio Calculations, Molecules 28 (1) (2023).
[43] R.N. Widmer, G.I. Lampronti, S. Chibani, C.W. Wilson, S. Anzellini, S. Farsang, A. K. Kleppe, N.P.M. Casati, S.G. MacLeod, S.A.T. Redfern, F.X. Coudert, T.D. Bennett, Rich Polymorphism of a Metal-Organic Framework in Pressure-Temperature Space, J. Am. Chem. Soc. 141 (23) (2019) 9330–9337.
[44] F. Colmenero, Silver oxalate: mechanical properties and extreme negative mechanical phenomena, Adv. Theor. Simul. 2 (6) (2019).
[45] F. Colmenero, X.X. Jiang, X.D. Li, Y.C. Li, Z.S. Lin, Negative area compressibility in silver oxalate, J. Mater. Sci. 56 (1) (2021) 269–277.
[46] F. Colmenero, V. Timon, ZIF-75 under pressure: negative linear compressibility and pressure-induced instability, Appl. Sci. -Basel 12 (20) (2022).
[47] F. Colmenero, Negative linear compressibility in nanoporous metal-organic frameworks rationalized by the empty channel structural mechanism, Phys. Chem. Chem. Phys. 23 (14) (2021) 8508–8524.
[48] P. Giannozzi, S. Baroni, N. Bonini, M. Calandra, R. Car, C. Cavazzoni, D. Ceresoli, G.L. Chiarotti, M. Cococcioni, I. Dabo, A. Dal Corso, S. de Gironcoli, S. Fabris, G. Fratesi, R. Gebauer, U. Gerstmann, C. Gougoussis, A. Kokalj, M. Lazzeri, L. Martin-Samos, N. Marzari, F. Mauri, R. Mazzarello, S. Paolini, A. Pasquarello, L. Paulatto, C. Sbraccia, S. Scandolo, G. Sclauzero, A.P. Seitsonen, A. Smogunov, P. Umari, R.M. Wentzcovitch, QUANTUM ESPRESSO: a modular and open-source software project for quantum simulations of materials, J. Phys. -Condens Mat. 21 (39) (2009).
[49] J.P. Perdew, K. Burke, M. Ernzerhof, Generalized gradient approximation made simple, Phys. Rev. Lett. 77 (18) (1996) 3865–3868.
[50] P.E. Blochl, Projector augmented-wave method, Phys. Rev. B 50 (24) (1994) 17953–17979.
[51] S. Grimme, Semiempirical GGA-type density functional constructed with a long-range dispersion correction, J. Comput. Chem. 27 (15) (2006) 1787–1799.
[52] S.R. Billeter, A.J. Turner, W. Thiel, Linear scaling geometry optimisation and transition state search in hybrid delocalised internal coordinates, Phys. Chem. Chem. Phys. 2 (10) (2000) 2177–2186.
[53] H.J. Monkhorst, J.D. Pack, Special points for Brillouin-zone integrations, Phys. Rev. B 13 (12) (1976) 5188–5192.
[54] A. Dal, Corso, Elastic constants of beryllium: a first-principles investigation, J. Phys. -Condens Mat. 28 (7) (2016).
[55] K. Momma, F. Izumi, VESTA 3 for three-dimensional visualization of crystal, volumetric and morphology data, J. Appl. Crystallogr 44 (2011) 1272–1276.
[56] A.L. Spek, Single-crystal structure validation with the program PLATON, J. Appl. Crystallogr 36 (2003) 7–13.
[57] R. Gaillac, P. Pullumbi, F.X. Coudert, ELATE: an open-source online application for analysis and visualization of elastic tensors, J. Phys. -Condens Mat. 28 (27) (2016).
[58] M.J. Cliffe, A.L. Goodwin, PASCal: a principal axis strain calculator for thermal expansion and compressibility determination, J. Appl. Crystallogr 45 (2012) 1321–1329.
[59] P. Hirel, Atomsk: A tool for manipulating and converting atomic data files, Comput. Phys. Commun. 197 (2015) 212–219.
[60] R.B. Fu, X.T. Wu, S.M. Hu, J.J. Zhang, Z.Y. Fu, W.X. Du, Crystal structures of five transition-metal 1,4-butylenediphosphonates, Polyhedron 22 (19) (2003) 2739–2744.
[61] J.S. Kim, H. Kim, M. Ree, Hydrothermal synthesis of single-crystalline zinc glutarate and its structural determination, Chem. Mater. 16 (16) (2004) 2981–2983.
[62] S. Klaus, M.W. Lehenmeier, E. Herdtweck, P. Deglmann, A.K. Ott, B. Rieger, Mechanistic Insights into Heterogeneous Zinc Dicarboxylates and Theoretical Considerations for CO_2-Epoxide Copolymerization, J. Am. Chem. Soc. 133 (33) (2011) 13151–13161.
[63] Q.X. Zeng, K. Wang, B. Zou, Abnormal compressive behaviors of metal-organic frameworks under hydrostatic pressure, Langmuir 38 (30) (2022) 9031–9036.
[64] X.X. Jiang, Y. Yang, M.S. Molokeev, P.F. Gong, F. Liang, S.H. Wang, L. Liu, X. Wu, X.D. Li, Y.C. Li, S.F. Wu, W. Li, Y.C. Wu, Z.S. Lin, Zero Linear Compressibility in Nondense Borates with a "Lu-Ban Stool"-Like Structure, Adv. Mater. 30 (32) (2018).
[65] Q.X. Zeng, W.B. Qiu, J. Hao, K. Wang, Y.W. Li, Tunable zero linear compressibility under a rational designed mechanism of modular "dumbbell": a density functional theory study, Acs Mater. Lett. 4 (4) (2022) 541–547.
[66] Z. Su, Y.R. Miao, G.H. Zhang, J.T. Miller, K.S. Suslick, Bond breakage under pressure in a metal organic framework, Chem. Sci. 8 (12) (2017) 8004–8011.
[67] S. Cao, T.D. Bennett, D.A. Keen, A.L. Goodwin, A.K. Cheetham, Amorphization of the prototypical zeolitic imidazolate framework ZIF-8 by ball-milling, Chem. Commun. 48 (63) (2012) 7805–7807.
[68] M. Erkartal, M. Durandurdu, Pressure-Induced Amorphization of MOF-5: A First Principles Study, Chemistryselect 3 (28) (2018) 8056–8063.
[69] Y.L. Gu, T. Kar, S. Scheiner, Fundamental properties of the CH center dot center dot center dot O interaction: Is it a true hydrogen bond? J. Am. Chem. Soc. 121 (40) (1999) 9411–9422.
[70] T. Steiner, C–H···O hydrogen bonding in crystals, Crystallogr. Rev. 9 (2–3) (2003) 177–228.
[71] R.A. Vergenz, I. Yazji, C. Whittington, J. Daw, K.T. Tran, Computational evidence for methyl-donated hydrogen bonds and hydrogen-bond networking in 1,2-ethanediol-dimethyl sulfoxide, J. Am. Chem. Soc. 125 (40) (2003) 12318–12327.
[72] P. Cysewski, Pressure-imposed changes of benzoic acid crystals, J. Mol. Model 21 (4) (2015).
[73] G. Jenner, Kinetic effects of high pressure in congested and strained molecular systems. A useful application of high pressure in organic synthesis, High. Press. Res 11 (1–3) (1993) 21–32.
[74] W.H. Xiao, Y. Yang, Z.P. Pi, F. Zhang, Phase Stability and Mechanical Properties of the Monoclinic, Monoclinic-Prime and Tetragonal REMO4 (M = Ta, Nb) from First-Principles Calculations, Coatings 12 (1) (2022).